Journal of Power Sources 199 (2012) 413–417

Contents lists available at SciVerse ScienceDirect

Journal of Power Sources

journal homepage: www.elsevier.com/locate/jpowsour

Short communication

Self-assembled synthesis of hierarchically porous NiO film and its application for electrochemical capacitors

Y.Q. Zhang, X.H. Xia, J.P. Tu*, Y.J. Mai, S.J. Shi, X.L. Wang, C.D. Gu.

State Key Laboratory of Silicon Materials and Department of Materials Science and Engineering, Zhejiang University, Hangzhou 310027, China

ARTICLE INFO

Article history:
Received 21 June 2011
Received in revised form 26 August 2011
Accepted 17 October 2011
Available online 20 October 2011

Keywords:
Nickel oxide
Electrochemical capacitor
Porous film

ABSTRACT

A hierarchically porous NiO film on nickel foam substrate is prepared by a facile ammonia-evaporation method. The self-assembled film possesses a structure consisting of NiO triangular prisms and randomly porous NiO nanoflakes. The pseudocapacitive behaviors of the porous NiO film are investigated by cyclic voltammograms and galvanostatic charge–discharge tests in 1 M KOH. The hierarchically porous NiO film exhibits a high discharge capacitance and excellent rate capability with 232 F g^{-1}, 229 F g^{-1}, 213 F g^{-1} and 200 F g^{-1} at 2, 4, 10, and 20 A g^{-1}, respectively. The specific capacitance of 87% is maintained from 2 A g^{-1} to 20 A g^{-1}. The porous NiO film also shows rather good cycling stability and exhibits a specific capacitance of 348 F g^{-1} after 4000 cycles.

1. Introduction

Electrochemical capacitors (ECs), also called supercapacitors, represent an emerging energy storage technology that offers high power density, long cycling life and fast recharge ability. ECs store energy using either ion adsorption (electrochemical double layer capacitors) or fast surface redox reactions (pseudo-capacitors) [1,2]. Redox-based ECs materials have shown the potential to combine the high energy density of conventional batteries and the high power capabilities of electrostatic capacitors [3]. Transition metal oxides such as RuO_2 [4–7], MnO_2 [8–11], Co_3O_4 [12–14] and NiO [15–17] are considered as the most promising pseudocapacitor candidate materials due to their high capacitances with several times larger than carbonaceous materials [18]. ECs based on RuO_2 are capable of delivering specific capacitance ranging from 720 to 860 F g^{-1} (for a single electrode system) [6]. However, apart from being toxic, RuO_2 is quite expensive for extensive commercial applications. Therefore, great efforts have been devoted to searching for inexpensive alternative materials with good capacitive characteristics similar to RuO_2.

Among the explored systems, NiO is of particular interest owing to its easy availability, cost effectiveness, and good pseudocapacitive behavior. There have been a variety of reports of the synthesis of different NiO nanostructures including porous nano/microspheres [19] nanoflowers [20,21], nanosheets or nanoflake [22–24], nanotubes [25,26] and nanofibers [27,28]. And it has been shown that their morphology plays an important role in capacitance enhancement. It is well accepted that pseudocapacitance is an interfacial phenomenon tightly related to the morphology of electroactive materials. The porous structure could provide a very short diffusion pathway for ions as well as large active surface area, leading to enhanced electrochemical properties [18,19,29,30]. Therefore, it is believed that the porous NiO film could exhibit superior pseudocapacitor performance. Recently, self-assembled synthesis of hierarchically structured NiO particles such as sandwich-like triangular NiO film has been developed [31]. Nevertheless, there is little literature into self-assembled synthesis of hierarchically porous NiO film and their application for ECs. Herein, we report a nickel foam-supported hierarchical NiO film consisting of triangular prisms NiO and randomly porous NiO nanoflakes. As a cathodic electrode material, the self-assembled NiO film exhibits superior pseudocapacitive performance with excellent capacity retention and high-rate capacity.

2. Experimental

All the reagents were analytical grade and were used without further purification. 30 ml aqueous ammonia (25–28%) was added to 30 ml aqueous solution of 0.1 M $Ni(NO_3)_2{\cdot}H_2O$ with vigorous stirring. Nickel foam substrate with a size of 2 cm × 3 cm was pressed to thin plate by 10 MPa and cleaned ultrasonically in ethanol for 10 min. Its top side was protected for solution contamination by uniformly coating with a polytetrafluoroethylene tape. Then, it was immersed into the reaction solution. After heated at 90 °C for 5 h, the nickel foam substrate was covered with a green film. This green precursor film was washed with deionized water for several times,

* Corresponding author. Tel.: +86 571 87952573; fax: +86 571 87952856.
E-mail addresses: tujp@zju.edu.cn (J.P. Tu), wangxl@zju.edu.cn (X.L. Wang).

0378-7753/$ – see front matter © 2011 Elsevier B.V. All rights reserved.
doi:10.1016/j.jpowsour.2011.10.065

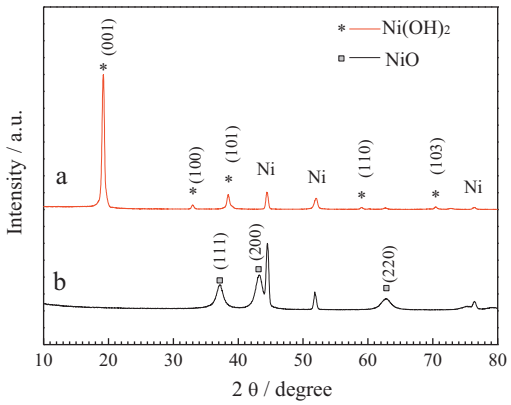

Fig. 1. XRD patterns of films (a) before and (b) after heat treatment.

and dried. Then the film was heated in a tube furnace at 300 °C for 2 h in flowing argon.

The structure and morphology of the film were characterized by X-ray diffraction (XRD, RigakuD/max-3B), scanning electron microscopy (SEM, D/Max-2550) and transmission electron microscopy (TEM, JEOL JEM200CX). The surface area of the film scratched from the substrate was determined by BET (Brunauer–Emmett–Teller) measurements using a NOVA-1000e surface area analyzer. Electrochemical measurements were carried out in a three-electrode electrochemical cell containing 1 M KOH aqueous solution as the electrolyte. Cyclic voltammetry (CV) measurements were performed on a CHI660c electrochemical workstation (Chenhua, Shanghai) at room temperature, with the NiO film as the working electrode, Hg/HgO as the reference electrode and a Pt foil as counter-electrode. The galvanostatic charge–discharge tests were conducted on a LAND battery program-control test system.

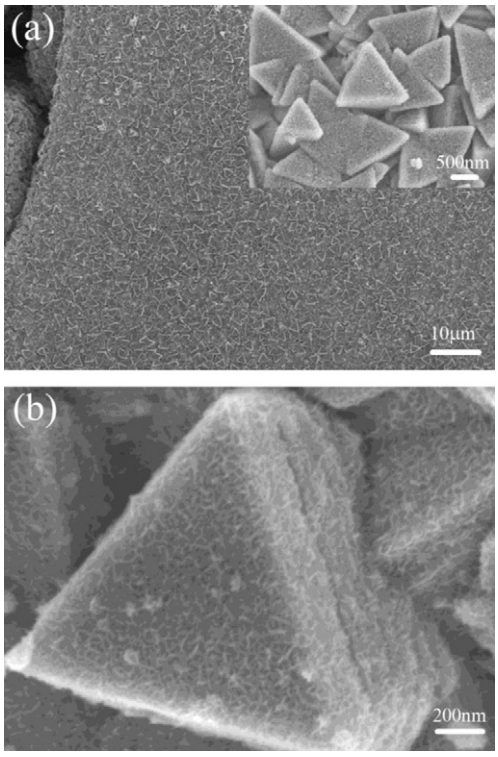

Fig. 2. SEM images of NiO film annealed at 300 °C for 2 h.

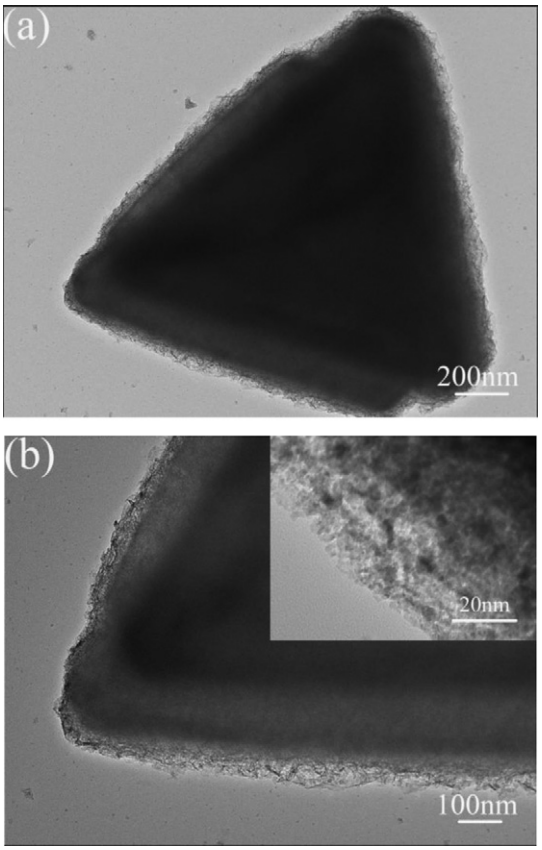

Fig. 3. TEM images of NiO film annealed at 300 °C for 2 h.

3. Results and discussion

XRD patterns of films before and after heat treatment are shown in Fig. 1. For the precursor film (pattern a), excluding three strong peaks from the nickel foam substrate, all the diffraction peaks correspond to well-crystallized β-phase hexagonal nickel hydroxide (JCPDS 14-0117). The diffraction peak at 19.3° indexed to (0 0 1) plane of β-Ni(OH)$_2$ is much stronger than the others. It implies that the preferable growth of β-Ni(OH)$_2$ along ⟨0 0 1⟩ direction. After annealing at 300 °C, the β-Ni(OH)$_2$ precursor film converts into NiO phase (JCPDS 47-1049) (pattern b).

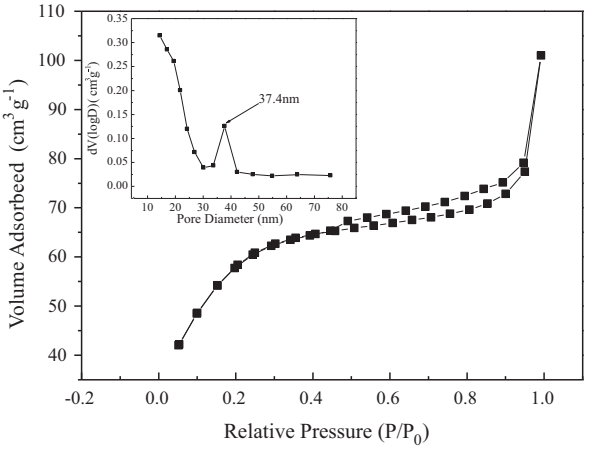

Fig. 4. BET isotherm of NiO film. The inset shows pore size distribution, calculated from desorption branch of isotherm, using BJH method.

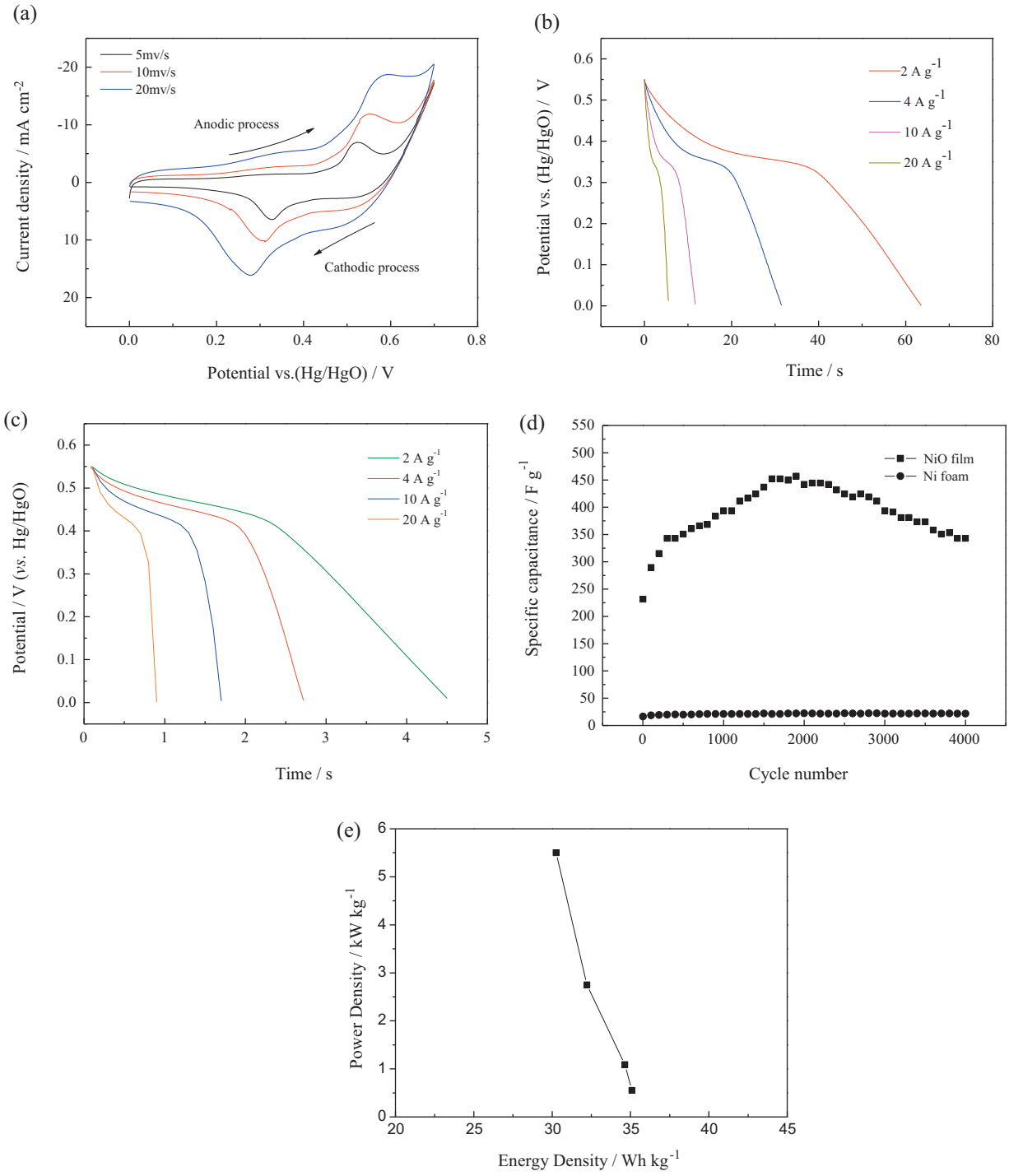

Fig. 5. Electrochemical characterizations of the hierarchically porous NiO film. (a) CV curves at different scan rates, (b) discharge curves of NiO film at different discharge current densities, (c) discharge curves of Ni foam at different discharge current densities, (d) cycling performance of NiO film and Ni foam at 2 A g^{-1}, (e) Ragone plots (Power density vs. energy density).

Fig. 2 shows SEM images of the as-prepared NiO film annealed at 300 °C for 2 h. Notice that the nickel foam substrate is fully covered by numerous homogeneous small triangular prisms (Fig. 2a). And the overall size of those triangular prisms is usually in the micron range. Interestingly, as shown in a magnified SEM image (Fig. 2b), each prism consists of two parts including regular stacking of triangular platelets and randomly porous NiO nanoflakes. These NiO nanoflakes grow vertically on the triangular platelets forming the porous surface. The special morphological characteristics are supported by TEM results. Obviously, the regular triangular platelets are uniformly decorated by nanoflakes with a thickness of approximately 100 nm (Fig. 3a). The individual nanoflake is composed of nanoparticles with diameters of 5–10 nm (Fig. 3b).

Formation of β-$Ni(OH)_2$ by ammonia-evaporation method has been studied in earlier works [18,31,32]. The formation of β-$Ni(OH)_2$ arises from the competition balance between reactions (1) and (2).

$$Ni^{2+} + 6NH_3 \rightarrow [Ni(NH_3)_6]^{2+} \quad (1)$$

$$[Ni(NH_3)_6]^{2+} + 2OH^- \xrightarrow{90\ ^\circ C} Ni(OH)_2 \downarrow + 6NH_3 \quad (2)$$

In a typical β-$Ni(OH)_2$ molecule, the metal cation Ni^{2+} is located in the central spaces of oxygen octahedral from six hydroxyl groups. These octahedral then share their edges to form two dimensional (2D) sheets. Ammonia plays the major role in controlling the hierarchically porous NiO film during the self-assembly growth process. The nanostructures grow in a dynamic process with a gradual decreasing of pH value and ammonia concentration in the solution. In the beginning, the high concentration of dissolved ammonia in the initial solution brings excess NH_4^+ and NH_3, reacting with Ni^{2+} to form $[Ni(NH_3)_6]^{2+}$. Ammonia begins to evaporate at 90 °C, and the hydrolysis of $[Ni(NH_3)_6]^{2+}$ occurs and leads to the formation of $Ni(OH)_2$ platelets. Under the function of ammonia, those platelets stack into triangular prism. When ammonia concentration decreases, the nanoflakes randomly grow on the triangular prisms. After annealing, the NiO keeps the hierarchically porous morphology of precursor $Ni(OH)_2$ film. In order to further investigate the hierarchically porous NiO film, a nitrogen adsorption–desorption technique was used. The N_2 adsorption–desorption isotherm of NiO is given in Fig. 4 with pore size distribution in the inset. The isotherm demonstrates the porous nature of NiO sample. According to Brunauer–Emmett–Teller (BET) analysis, a total specific surface area of 196.8 $m^2\,g^{-1}$ is obtained. The pore size distribution suggests that the NiO film synthesized by ammonia-evaporation method contains a distribution of macropores in the range of 33–42 nm, which is similar to that obtained from SEM. The hierarchical structure provides larger surface area and more active sites for electrochemical reactions.

The electrochemical performance of the hierarchically porous NiO film is elucidated by means of CV and galvanostatic charge–discharge in 1 M KOH aqueous solution. For NiO as an electrode material, it is well accepted that the surface faradaic reaction can be expressed as follows:

$$NiO + OH^- \leftrightarrow NiOOH + e^- \quad (3)$$

A pair of cathodic and anodic peaks is clearly observed in the CV curves (Fig. 5a). The charge process of the film is associated with the oxidation peak, whereas the discharge process is associated with the reduction peak. It indicates that the capacity mainly results from the pseudo-capacitance, which is based on a redox mechanism [21,26,33]. With the increase of sweep rate, the shape of the CV curve changes. The anodic and cathodic peak potentials shift in more anodic and cathodic directions, respectively, and the capacitance decreases inevitably, which is further confirmed by the result at different discharge current densities (Fig. 5b).

In practice, the ability to discharge at high rate is crucial in capacitors. The specific capacitances C_s are calculated from the first discharge curves using the following equation:

$$C = \frac{i\Delta t}{m\Delta V} \quad (4)$$

where C ($F\,g^{-1}$) is specific capacitance, i (mA) represents the current applied and m (mg), ΔV (V) and Δt (s) designate the mass of the active materials, potential drop during discharge and total discharge time, respectively. In this way, the specific capacitance of the porous NiO film at a galvanostatic current density of 2, 4, 10, and 20 $A\,g^{-1}$ are 232 $F\,g^{-1}$, 229 $F\,g^{-1}$, 213 $F\,g^{-1}$ and 200 $F\,g^{-1}$, respectively (Fig. 5b). The pseudocapacitances are obtained by subtracting the discharge time of nickel foam. And as shown in Fig. 5c, the nickel foam only exhibits small capacitance with several discharge seconds.

The rate capability is another important factor required for practical applications. 87% of capacitance is retained when the current density changes from 2 $A\,g^{-1}$ to 20 $A\,g^{-1}$. It is much higher than the result obtained by Song et al. [21], only 41.56% capacitance is retained from 2 $A\,g^{-1}$ to 10 $A\,g^{-1}$. The excellent rate capability is mainly attributed to the following two reasons: first, the porous NiO nanoflakes on triangular prisms provide a large specific surface area for electrolyte access and shortens the diffusion path in solid phase, resulting in fast redox reactions. Second, every prism grows directly on the foam nickel substrate, which can enhance the conductivity of the electrode.

Fig. 5d shows the cyclability of the hierarchically porous NiO film and the NiO film substrate over 4000 cycles between 0 and 0.55 V at a discharging current of 2 $A\,g^{-1}$. The porous-structured NiO electrode shows an obvious increase in the specific capacitance, from 232 $F\,g^{-1}$ to 349 $F\,g^{-1}$, during the first 400 cycles, and then a slight increase to the highest specific capacitance (441 $F\,g^{-1}$) until around 1500 cycles. This phenomenon might be attributed to the hierarchically porous structure. The first obvious increase of capacitance should be the activation process of the randomly porous NiO nanoflakes and the surface of triangular prisms. The activation process of inner active material of triangular prism leads to later slight increase. In other words, the electrolyte gradually penetrates into the internal of NiO, and then the inner active materials participate in the electrical reaction. After 4000 cycles the hierarchically porous NiO electrode exhibits excellent specific capacitance retention with 348 $F\,g^{-1}$. Our values are higher than those obtained from the electrodeposited nanoporous NiO films (<200 $F\,g^{-1}$) [29,34], and comparable to mesoporous NiO film (327 $F\,g^{-1}$) [35], and macroporous NiO film (351 $F\,g^{-1}$) [36]. The capacitance of Ni foam substrate increases from 16.3 $F\,g^{-1}$ to 20.2 $F\,g^{-1}$ around 400 cycles, then increases to 21 $F\,g^{-1}$ and 23.5 $F\,g^{-1}$ at 1500 cycles and 4000 cycles, respectively. It indicates that the increased specific capacitance mostly is due to the activation process of the active material. Fig. 5e shows the Ragone plots (Power density vs. energy density) of the hierarchically porous NiO film. The energy and power densities were derived from the discharge curves of NiO film at different discharge current densities. Our NiO film delivered a high energy density of about 30 Wh kg^{-1} at a high power density of 5.5 kW kg^{-1}. Based on these results, it is believed that the hierarchically porous NiO is a good electrode material for supercapacitors.

4. Conclusions

In summary, a hierarchically porous NiO film directly grown on nickel foam substrate is prepared by a facile ammonia-evaporation method. The film possesses a structure consisting of NiO triangular prisms and randomly porous NiO nanoflakes. The high specific capacitance and remarkable rate capability are promising for applications in supercapacitors with both high energy and power densities. The enhanced electrochemical capacitance is mainly due to its hierarchically porous structure.

Acknowledgement

The authors would like to acknowledge financial support from China Postdoctoral Science Foundation (Grant No. 20100481401).

References

[1] P. Simon, Y. Gogotsi, Nat. Mater. 7 (2008) 845.
[2] Y. Zhang, H. Feng, X.B. Wu, L.Z. Wang, A.Q. Zhang, T.C. Xia, H.C. Dong, X.F. Li, L.S. Zhang, Int. J. Hydrogen Energy 34 (2009) 4889.
[3] X. Zhao, B.M. Sanchez, P.J. Dobson, P.S. Grant, Nanoscale 3 (2011) 839.
[4] R.R. Bi, X.L. Wu, F.F. Cao, L.Y. Jiang, Y.G. Guo, L.J. Wan, J. Phys. Chem. C 114 (2010) 2448.
[5] C.C. Hu, K.H. Chang, M.C. Lin, Y.T. Wu, Nano Lett. 6 (2006) 2690.
[6] J.T. Zhang, J.Z. Ma, L.L. Zhang, P.Z. Guo, J.W. Jiang, X.S. Zhao, J. Phys. Chem. C 114 (2010) 13608.
[7] A. Devadas, S. Baranton, T.W. Napporn, C. Coutanceau, J. Power Sources 196 (2011) 4044.
[8] X.L. Wang, A.B. Yuan, Y.Q. Wang, J. Power Sources 172 (2007) 1007.

[9] Q. Lu, Y.K. Zhou, J. Power Sources 196 (2011) 4088.
[10] R.R. Jiang, T. Huang, J.L. Liu, J.H. Zhuang, A.S. Yu, Electrochim. Acta 54 (2009) 3047.
[11] R. Amade, E. Jover, B. Caglar, T. Mutlu, E. Bertran, J. Power Sources 196 (2011) 5779.
[12] X.H. Xia, J.P. Tu, X.L. Wang, C.D. Gu, X.B. Zhao, Chem. Commun. 47 (2011) 5786.
[13] T. Zhu, J.S. Chen, X.W. Lou, J. Mater. Chem. 20 (2010) 7015.
[14] X.H. Xia, J.P. Tu, Y.J. Mai, X.L. Wang, C.D. Gu, X.B. Zhao, J. Mater. Chem. 21 (2011) 9319.
[15] A.I. Inamdar, Y. Kim, S.M. Pawar, J.H. Kim, H. Im, H. Kim, J. Power Sources 196 (2011) 2393.
[16] D.W. Wang, F. Li, H.M. Cheng, J. Power Sources 185 (2008) 1563.
[17] D.C. Wang, W.B. Ni, H. Pang, Q.Y. Lu, Z.J. Huang, J.W. Zhao, Electrochim. Acta 55 (2010) 6830.
[18] X.H. Xia, J.P. Tu, X.L. Wang, C.D. Gu, X.B. Zhao, J. Mater. Chem. 21 (2011) 671.
[19] S.K. Meher, P. Justin, G.R. Rao, Electrochim. Acta 55 (2010) 8388.
[20] J.W. Lang, L.B. Kong, W.J. Wu, Y.C. Luo, L. Kang, Chem. Commun. (2008) 4213.
[21] C.Y. Cao, W. Guo, Z.M. Cui, W.G. Song, W. Cai, J. Mater. Chem. 21 (2011) 3204.
[22] Y.J. Mai, J.P. Tu, X.H. Xia, C.D. Gu, X.L. Wang, J. Power Sources 196 (2011) 6388.
[23] L. Liu, Y. Li, S.M. Yuan, M. Ge, M.M. Ren, C.S. Sun, Z. Zhou, J. Phys. Chem. C 114 (2010) 251.
[24] X.H. Huang, J.P. Tu, X.H. Xia, X.L. Wang, J.Y. Xiang, Electrochem. Commun. 10 (2008) 1288.
[25] S.A. Needham, G.X. Wang, H.K. Liu, J. Power Sources 159 (2006) 254.
[26] J.H. Kim, K. Zhu, Y.F. Yan, C.L. Perkins, A.J. Frank, Nano Lett. 10 (2010) 4099.
[27] Y.J. Qiu, J. Yu, X.S. Zhou, C.L. Tan, J. Yin, Nanoscale Res. Lett. 4 (2009) 173.
[28] M.M. Shaijumon, F.S. Ou, L.J. Ci, P.M. Ajayan, Chem. Commun. (2008) 2373.
[29] M.S. Wu, Y.A. Huang, C.H. Yang, H.H. Jow, Int. J. Hydrogen Energy 32 (2007) 4153.
[30] X.H. Xia, J.P. Tu, J. Zhang, X.H. Huang, X.L. Wang, W.K. Zhang, H. Huang, Electrochem. Commun. 10 (2008) 1815.
[31] J. Zhong, X.L. Wang, X.H. Xia, C.D. Gu, J.Y. Xiang, J. Zhang, J.P. Tu, J. Alloys Compd. 509 (2011) 3889.
[32] D.B. Kuang, B.X. Lei, Y.P. Pan, X.Y. Yu, C.Y. Su, J. Phys. Chem. C 113 (2009) 5508.
[33] T. Nathan, A. Aziz, A.F. Noor, S.R.S. Prabaharan, J. Solid State Electrochem. 12 (2008) 1003.
[34] M.S. Wu, C.Y. Huang, K.H. Lin, J. Power Sources 186 (2009) 557.
[35] H.L. Li, M.W. Xu, S.J. Bao, J. Solid State Electrochem. 11 (2007) 372.
[36] M.S. Wu, M.J. Wang, J.J. Jow, J Power Sources 195 (2010) 3950.